

Electronic Supplementary information for

High-power graphene supercapacitors for effective storage of regenerative energy during braking and deceleration process in electric vehicles

Sindhuja Manoharan¹, Karthikeyan Krishnamoorthy¹, Arunprasath Sathyaseelan¹,

Sang-Jae Kim^{1, 2, 3 *}

¹Nanomaterials & System Laboratory, Major of Mechatronics Engineering,
Faculty of Applied Energy System, Jeju National University, Jeju 63243, Republic of Korea.

²Semiconductor & Display Research Centre, Jeju National University,
Jeju 63243, Republic of Korea

³Research Institute of Advanced Technology, Jeju National University,
Jeju 63243, Republic of Korea

*Corresponding author email id.: kimsangj@jejunu.ac.kr

S1. Materials and methods:

S1.1 Materials.

Graphite powder (lateral size less < 20 μm) was obtained from Sigma–Aldrich, South Korea. Sulphuric acid, potassium permanganate, hydrochloric acid and hydrogen peroxide were purchased from Daejung Chemicals and Metal Ltd., South Korea. A SONIC VCX 750 model (20 kHz, 750 W) with a direct immersion titanium horn was used for the ultrasound irradiation process.

S1.2 Preparation of graphene oxide sheets.

The GO sheets were prepared by the oxidation of graphite in accordance with the modified Hummers method using potassium permanganate and hydrochloric acid followed by ultrasonication process¹. Briefly, graphite powders (2 g) were immersed in a solution containing sulphuric acid (60 mL) and allowed to mechanical stirring process for 3 h. Then, 6 g of potassium permanganate (oxidizer) was gradually added to the solution containing graphite and sulphuric acid and the stirring process was continued for 4 h. After this, the resulting solution was diluted via the addition of water (100 mL) under vigorous stirring. Then, the suspension was further treated by the addition of 30% H_2O_2 solution (10 mL) and 150 mL of distilled water. The resulting graphite oxide powders was collected after by repeated centrifugation using 5% HCl, and water until the pH of the solution became neutral. The exfoliation of graphitic oxide into a GO sheets were achieved via subjecting the graphite oxide dispersion under ultrasound irradiation for 1 h. Finally, the GO sheets were obtained via filtration process and allowed to dry at room temperature.

S1.3 Thermal reduction of graphene oxide into graphene sheets.

The graphene sheets were prepared via thermal reduction of GO sheets at high temperature. Briefly, 1 g of as GO sheets was well grounded and annealed at a temperature

900 °C (with a heating rate of 10 °C) for 3 h in an Ar atmosphere, followed by cooling to room temperature. A black greyish powder was formed as a result of thermal reduction of GO sheets. The obtained graphene sheets were collected and used for further characterization.

S1.4 Instrumentation.

The phase purity and crystallinity of GO and graphene sheets were inspected using X-ray diffractometer (Rigaku) equipped with Cu K α radiation (40 KeV and 40mA). The laser Raman spectrum of GO and graphene sheets were analyzed using LabRam HR Evolution Raman spectrometer, Horiba Jobin-Yvon, France (power-10 mW; excitation wavelength -514 nm; the data-point acquisition time was 10 s). The Raman mapping of the graphene was performed over an area of $-2 \times 2 \mu\text{m}^2$ comprising 100 spectral arrays and are analyzed using LabSpec (Ver. 6.2) software. The surface morphology and elemental mapping of graphene sheets were examined by Field emission scanning electron microscopy using JSM6700F, JEOL Instruments. The chemical state of elements present in the graphene was analyzed using X-ray photoelectron spectroscopy with ESCA-2000, VG Microtech Ltd.

S1.5 Fabrication of graphene supercapacitors.

The graphene electrodes were fabricated using the standard slurry coating method widely used in literature with a ratio of graphene:PVDF binder of about 95:5². The graphene SC was fabricated with a CR2032 coin-cell configuration using graphene-coated stainless-steel substrates with area of 1.86 cm² as electrodes separated by a Celgard membrane and 1 M TEABF₄ in acetonitrile as the electrolyte. An electric coin cell crimping and disassembling machine (MTI, South Korea) was used to fabricate the graphene SC. The handling of electrolyte and fabrication of SC were carried inside a glove box with less than 1 ppm of moisture and oxygen.

S1.6 Testing of graphene supercapacitors and performance evaluation.

The charge-storage and delivery properties of the fabricated graphene SC were analyzed using studies such as (i) cyclic voltammograms (CV) recorded at different scan rates, (ii) electrochemical impedance spectroscopy (EIS) analysis recorded over the frequency range from 0.01 Hz to 100 kHz at an amplitude of 10 mV, and (iii) galvanostatic charge-discharge (CD) measurements in different applied current ranges. The long-term cyclic stability of the fabricated graphene SC was performed using continuous charge-discharge cycles using an applied current of 5 mA over 10,000 cycles. The temperature-dependent performance metrics of the graphene SC were determined by placing the SC in an electric oven (from 20 to 80 °C), refrigerator (5 °C), and freezer (-15 °C). All the electrochemical tests were carried out using an Autolab PGSTAT302N electrochemical workstation. The performance metrics of the graphene SCs such as the electrode capacitance (C_E), device capacitance (C_{SC}), energy density (E), and power density (P), were calculated from the CD analysis using the following relations³:

$$C_{SC} = (I \times T_D) / (M \times \Delta V) \dots\dots\dots (1)$$

$$C_E = 4 \times C_{SC} \dots\dots\dots (2)$$

$$E = [C_{SC} \times \Delta V^2] / 2 \dots\dots\dots (3)$$

$$P = E / T_D \dots\dots\dots (4)$$

Here, “ ΔV ” is the voltage window of the SC, “ I ” is the discharge current, “ M ” is the electroactive mass loading of graphene in the SC, and “ T_D ” is the time taken for discharge from maximum to minimum voltage. The specific capacitance of graphene SC with respect to applied frequency is derived from the EIS analysis using the relation ⁴:

$$C = 1 / (2\pi f z'') \dots\dots\dots (5)$$

Here “ C ” is the capacitance of the device, and “ f ” is the applied frequency, and “ z'' ” is the imaginary part of impedance. The real (C') and imaginary capacitance (C'') values were derived from the EIS analysis using the following relations ⁵:

$$C'_{\omega} = -Z''_{\omega} / (\omega |Z_{\omega}|^2) \dots\dots\dots (6)$$

$$C''_{\omega} = Z'_{\omega} / (\omega |Z_{\omega}|^2) \dots\dots\dots (7)$$

S1.6 Self-discharge analysis of graphene supercapacitors

The self-discharge properties of the graphene SCs were measured using a similar method reported in literature⁶. Here, the graphene SC was kept at required voltage maximum (V= 1, 2, and 3.0 V) for 10 minutes (voltage hold time) followed by the monitoring the self-discharge profiles.

S1.7 Graphene supercapacitors for applications in Electric Vehicles

A commercially available regenerative braking kit (prototype of EVs) obtained from Nevons Project, Ltd., (See Figure S13) India is used to analyze the applicability of graphene SC in EVs. Three graphene SCs connected in parallel is used as an auxiliary power source with commercial batteries (model) to drive EV prototype were demonstrated using the circuit design given in Figure S14. Figure S15 depicts the circuit used for assessment of regenerative braking and deceleration energy. Initially, the wheels of the EV prototype connected to DC motor was powered by a commercial battery and allowed to switch off after 1 minutes that leads to the deceleration for few seconds. The ability of a single graphene SC to store the deceleration energy monitored on Autolab PGSTAT302N electrochemical workstation.

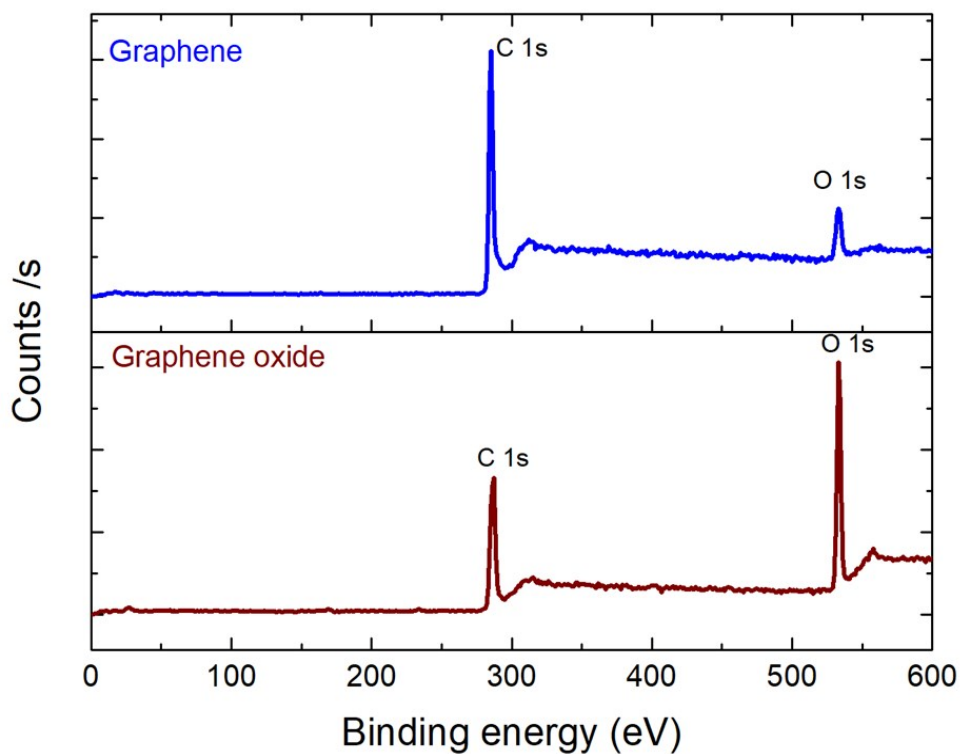


Figure S1. X-ray photoelectron survey spectra of graphene oxide and graphene sheets.

Figure S1 shows the X-ray photoelectron survey scan of graphene oxide (GO) and graphene sheets which reveals the presence of carbon and oxygen contents in the prepared materials. The survey spectrum of graphene shows higher content of carbon (C1s) compared to that of the GO. In addition, the oxygen content is reduced in the graphene to that of GO which confirms the reduction of GO to graphene sheets which is concordant with the previous reports.

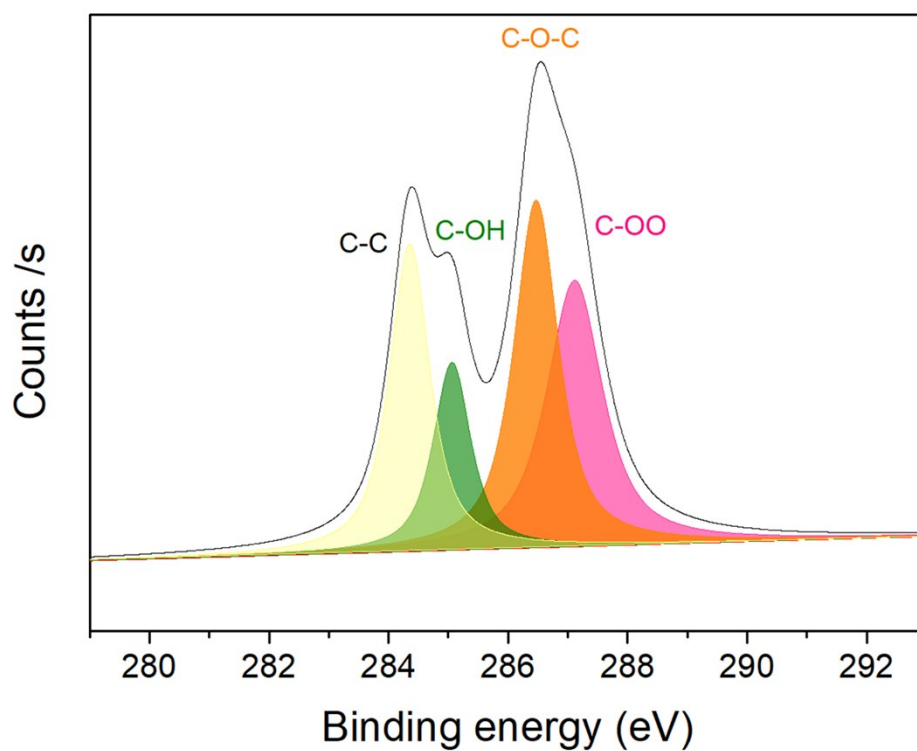


Figure S2 X-ray photoelectron core-level spectrum of C1s present in graphene oxide.

Figure S2 shows the XPS core-level spectrum of C1s present in the graphene oxide. The deconvolution of the C1s spectrum shows the presence of functional groups such as C-C, C-O, C-O-C and C=O, groups at the binding energy of 284.5, 285.6, 287.5, 288.9 eV, as a result of oxidation of graphite via Hummers method⁷.

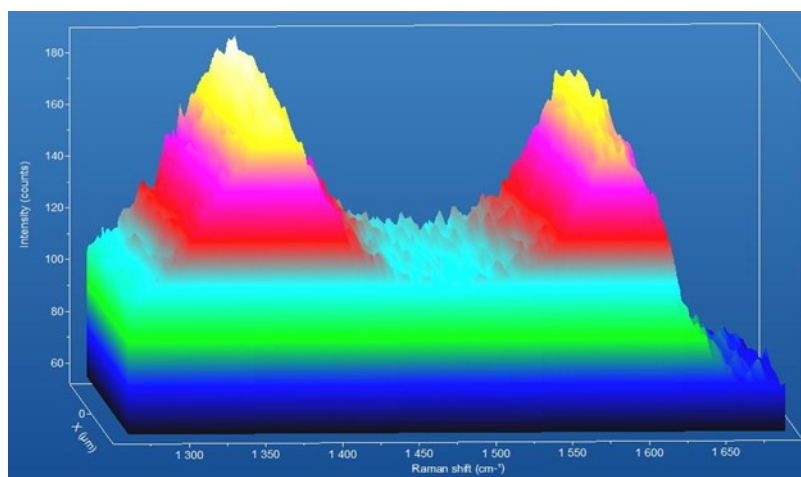


Figure S3. Laser Raman 3D spectrum of map of the graphene sheets.

Figure S3 shows the laser Raman 3D spectral map of the graphene sheets which reveals the presence of the D band and G band present in the graphene sheets.

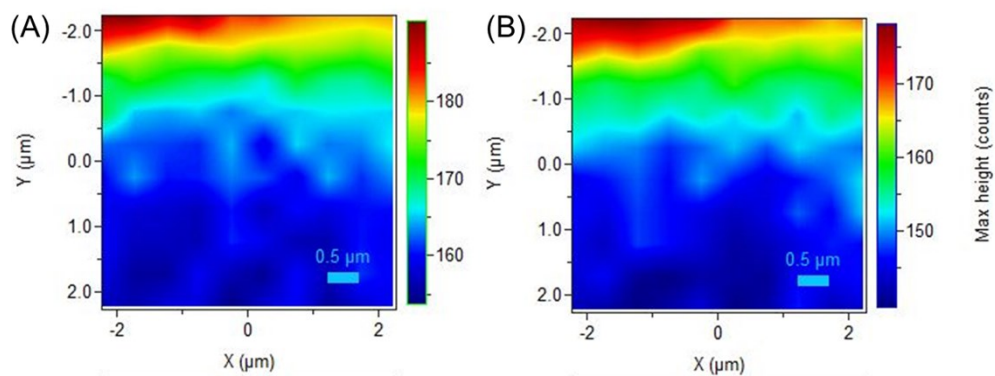


Figure S4 Laser Raman height map of (A) D band and (B) G band present in graphene sheets.

Figure S4 shows the laser Raman height maps of the D band and G band present in the graphene sheets mapped over an area of $-2 \times 2 \mu\text{m}$.

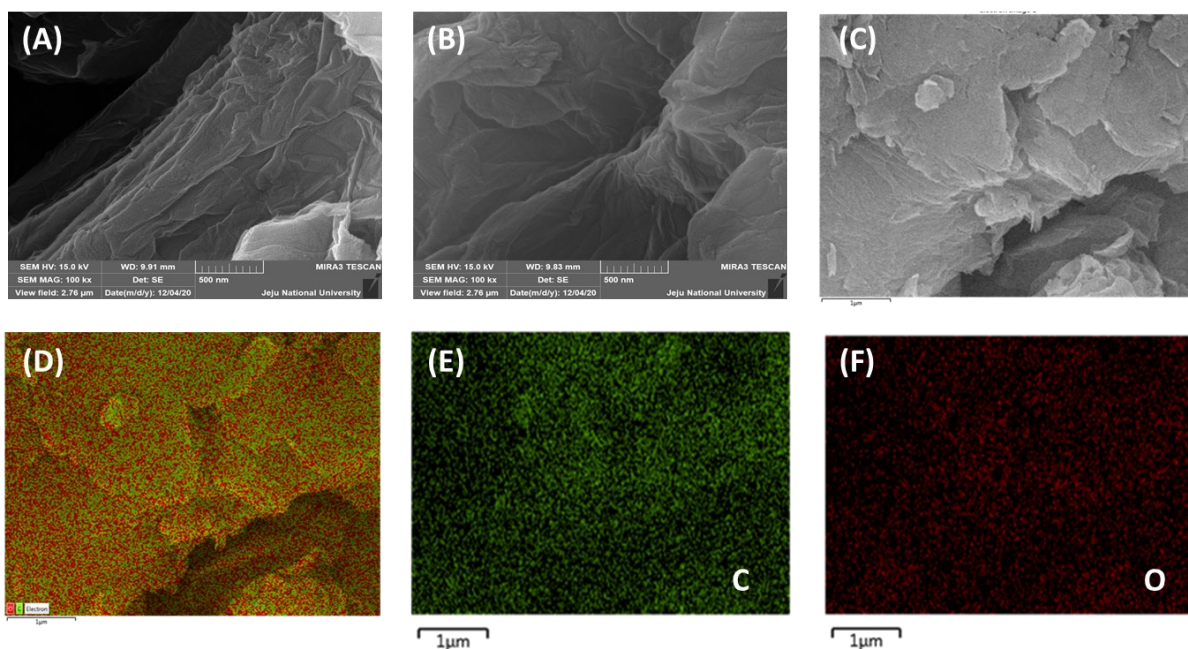


Figure S5. (A-B) Field emission scanning electron microscopic images of the graphene oxide. (C-D) overlay field emission scanning electron micrograph of the graphene oxide sheets. The elemental mapping analysis of (E) C and (F) O atoms present in the graphene oxide sheets.

Figure S5 (A-B) shows the FESEM micrograph of GO revealing the presence of layered structures suggesting the sheet like morphology. The elemental mapping analysis of the GO sheets using field emission scanning electron microscope (FE-SEM) provided in Figure S5 (E-F) indicating uniform distribution of carbon and oxygen atoms throughout the graphene oxide sheets.

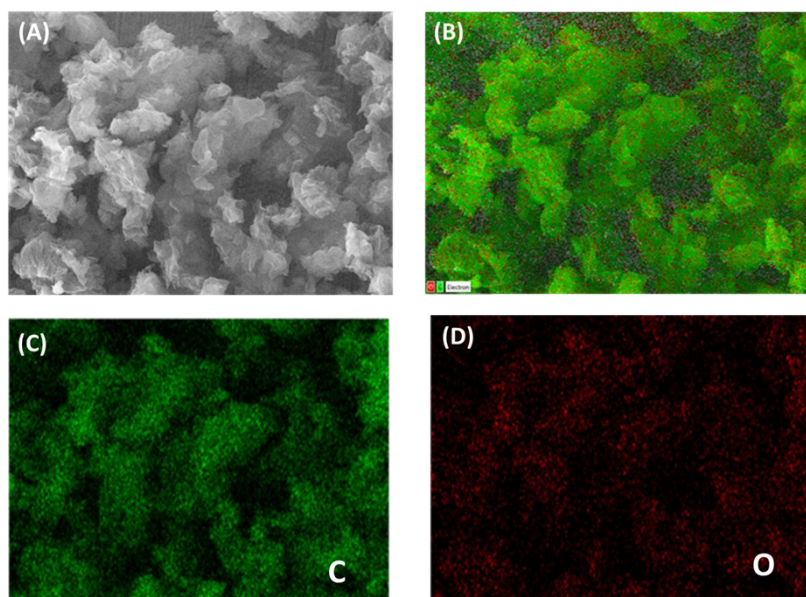


Figure S6. (A-B) overlay field emission scanning electron micrograph of the graphene sheets. The elemental mapping analysis of (C) C and (D) O atoms present in the graphene sheets.

Figure S6 (A-B) shows the overlay FESEM micrograph of graphene revealing the presence of sheet like structures. The elemental mapping analysis of the graphene sheets using field emission scanning electron microscope (FE-SEM) provided in Figure S6(C-D) indicating uniform distribution of carbon and oxygen atoms throughout the graphene sheets.

Element	Weight%	Atomic%
C K	89.67	92.04
O K	10.33	7.96
Totals	100.00	

Figure S7. EDS spectrum of graphene sheets.

Figure S7 shows the EDS spectrum of graphene sheets with the C:O atomic ratio of about 92.04:7.96 analyzed using Cliff–Lorimer ratio method⁴.

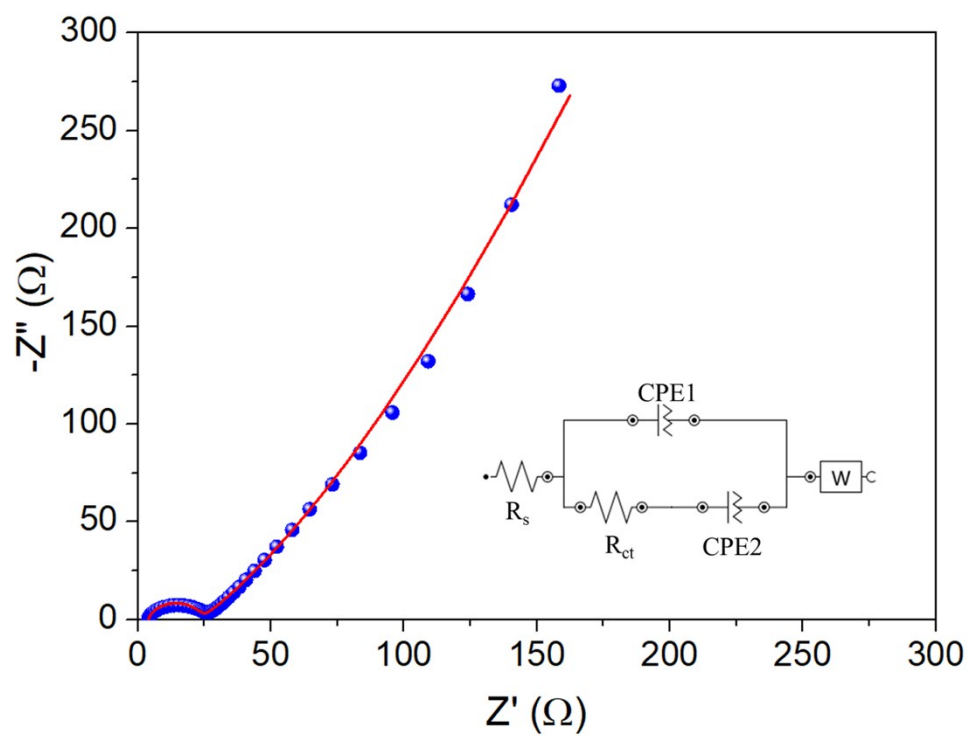


Figure S8. Nyquist plot of the graphene SC recorded at room temperature. The inset shows the equivalent circuit model for the graphene SC.

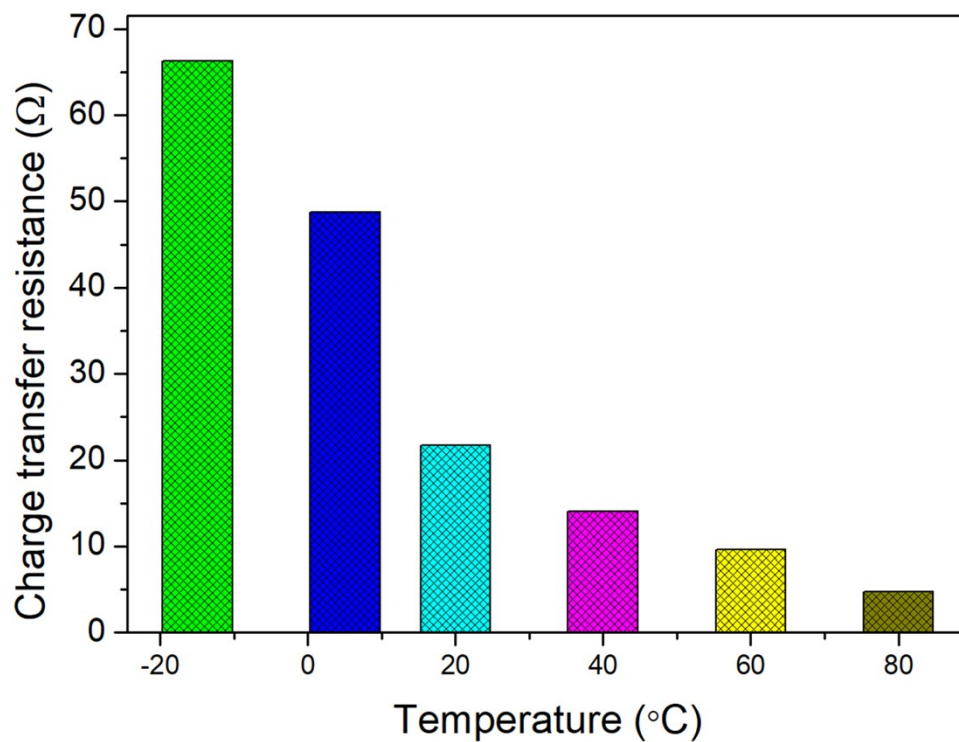


Figure S9. Plot of the charge-transfer resistance of the graphene SC with respect to applied temperature.

Figure S9 shows the plot of the charge transfer resistance of the graphene SC versus the applied temperature. Figure S9 indicates that the R_{ct} values of the graphene SC is higher at low temperature which is due to the limited ion-transport at these temperature range (-15 to 5 °C) and it decreases with an increase in temperatures (20 to 80 °C) due to the fast ion-transportation activated by the thermal energy^{8,9}.

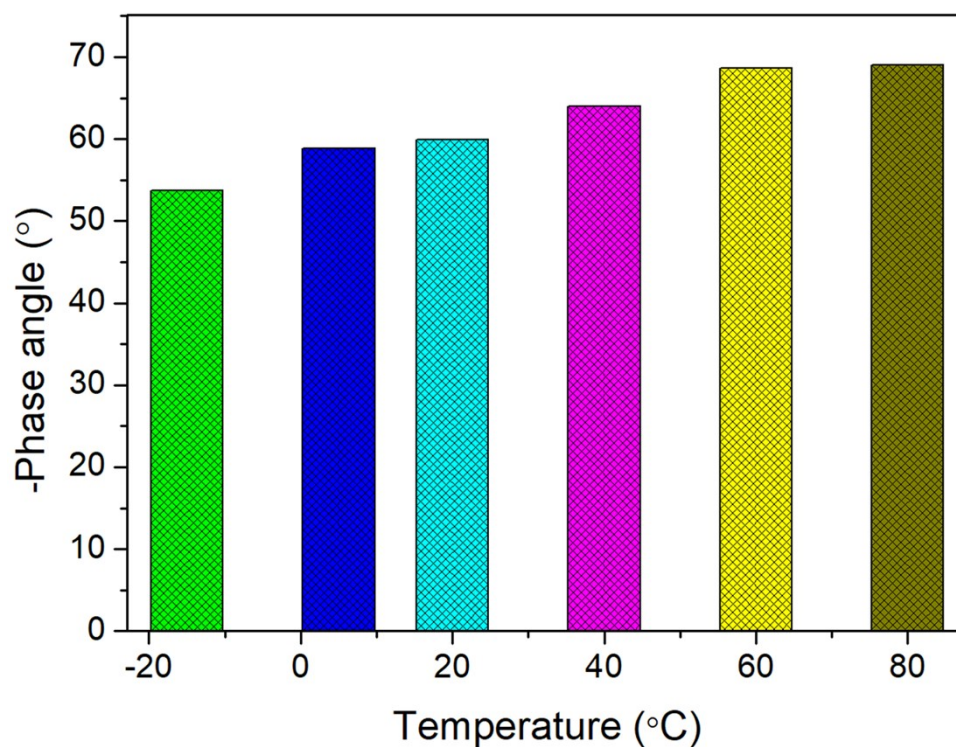


Figure S10. Plot of the Phase angle of the graphene SC with respect to applied temperature.

Figure S10 shows the Bode phase angle of the graphene SC at different temperature ranges reveals that the phase angle at a low frequency of 0.01 Hz is about 69.07° (closer to that of ideal capacitive nature¹⁰ is obtained at a temperature of 80 °C. The phase angle of the graphene SC decreases with decrease in temperature and reaches to a value of 53.69° temperature of -15 °C.

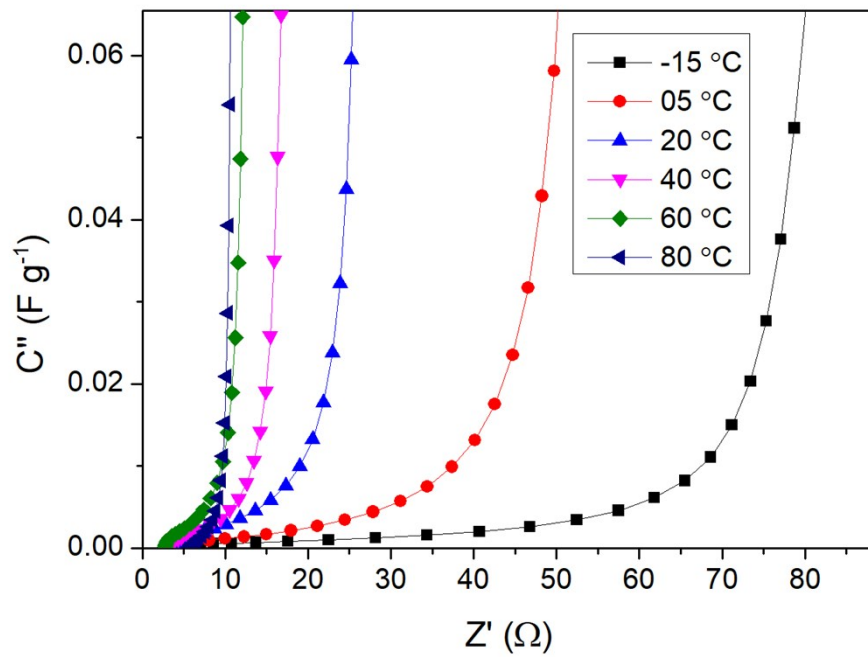


Figure S11. Enlarged portion of the C'' vs Z' graph (given in Figure 5(I)) at the high frequency regime.

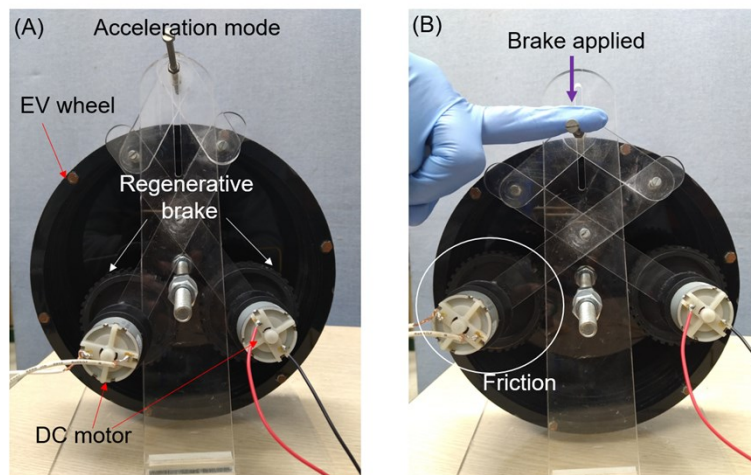


Figure S12. Regenerative braking kit in which (A) shows the acceleration or normal mode and (B) presents the braking mode.

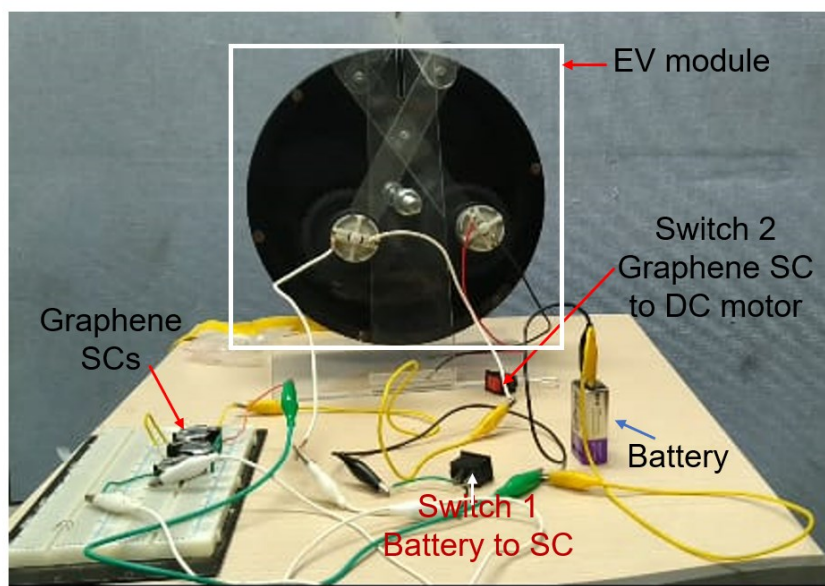


Figure S13. Digital photograph of the experimental setup used to analyze the use of three graphene SC as an auxiliary power source in combination with commercial battery for EVs.

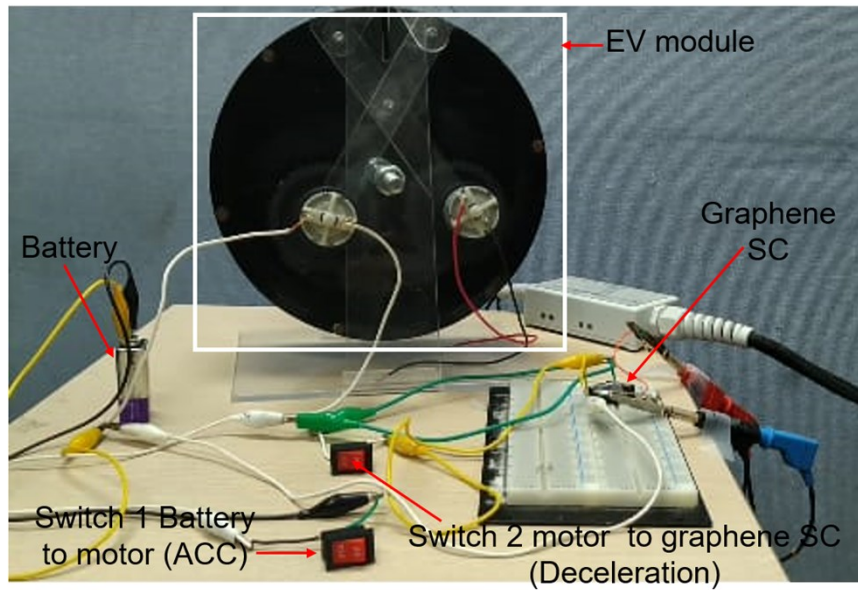


Figure S14. Digital photograph of the experimental setup used to analyze the efficiency of single graphene SC to capture the deceleration energy from EVs.

Table S1. Comparative performance metrics of graphene SSC to that of reported ionic/organic electrolyte SCs utilizing carbon, and graphene as electrodes.

S. No.	Electrodes for SC	Electrolyte	Voltage window (V)	Capacitance (F g ⁻¹)	Energy density (Wh kg ⁻¹)	Power density (W kg ⁻¹)	Ref
1	Activated carbon	BMPY-TFSI	0.0 to 3.0	16.3	25	5000	11
2	Super 30, Norit	Azp ₁₆ TFSI	0.0 to 3.5	-	19	~1700	12
3	Porous graphene macrofoam	TEABF ₄	0.0 to 2.5	26.5	23.5	312	13
4	Graphene / V ₂ O ₅	LiClO ₄ /PC	0.0 to 2.5	31.2	10.92	1034	14
5	Porous carbon	EMI-BF ₄	0.0 to 2.0	36.75	27.3	~7000	15
6	Poly (ionic liquid)-modified RGO	[MPPy] [TFSI]	0.0 to 3.0	16.07	40	2100	16
7	BDA/rGO	TEABF ₄	0.0 to 2.5	33.5	34	10000	17
8	Tris-rGO	TEABF ₄	0.0 to 3.5	29.75	32	1000	17
9	Graphene–CMK-5	LiPF ₆	0.0 to 2.3	~37	23.1	-	18
10	Graphene sheets	BMIMBF ₄	0.0 to 4.0 V	18.5	16.5	1600	19
11	Reduced graphene oxide	[SET ₃] [TFSI] / GO	0.0 to 2.5	25.9	17.7	875	20
12	Hydrothermally prepared rGO	TEABF ₄	0.0 to 3.0	28.46	35.58	7500	7
13	Sonochemically prepared rGO	TEABF ₄	0.0 to 3.0	30.46	38.07	15000	21
14	Graphene	TEABF ₄	0.0 to 3.0	35.96	44.95	18750	This work

Table S2. Comparative performance metrics of graphene SSC to that of reported ionic/organic electrolyte based SCs using 2D materials beyond graphene.

S. No.	Electrodes for SC	Electrolyte	Voltage window (V)	Capacitance (F g ⁻¹)	Energy density (Wh kg ⁻¹)	Power density (W kg ⁻¹)	Ref
1	ReS ₂	TEABF ₄	0.0 to 2.0	51.4	28.5	10000	22
2	MoS ₂	TEABF ₄	0.0 to 3.0	24.98	20.68	1858.64	23
3	MoS ₃	TEABF ₄	0.0 to 3.0	6.3	3.39	790.98	23
4	MoSe ₂	TEABF ₄	0.0 to 3.0	25.31	20.31	7500	24
5	Siloxene	TEABF ₄	0.0 to 3.0	4.06	5.08	8000	4
6	Blue TiO ₂ Sheets	TEABF ₄	0.0 to 3.0	4.8	6	15000	25
7	Carbon/siloxene/Ni	TEABF ₄	0.0 to 3.0	24.65	30.81	15625	26
8	Reduced oxygen defective boron nanosheet	BMIMBF ₄	0.0 to 3.0	22.24	25.1	636.1	27
9	Silicon oxy carbide	TEABF ₄	0.0 to 3.0 V	16.7	20.89	750	3
10	Boron-oxy carbide	TEABF ₄	0.0 to 2.0 V	11.6	6.25	150	28
11	Maxwell	-	2.7	-	2.5	11390	29
12	Ness	-	2.7	-	3.6	8674	29
13	Panoasonic	-	2.5	-	3.44	16800	29
14	APowerCap	-	2.7	-	5.0	8300	29
15	Graphene	TEABF ₄	0.0 to 3.0	35.96	44.95	18750	This work

References

- 1 K. Krishnamoorthy, M. Veerapandian, K. Yun and S. J. Kim, The chemical and structural analysis of graphene oxide with different degrees of oxidation, *Carbon N. Y.*, 2013, **53**, 38–49.
- 2 K. Krishnamoorthy, P. Pazhamalai, V. K. Mariappan, S. S. Nardekar, S. Sahoo and S.-J. Kim, Probing the energy conversion process in piezoelectric-driven electrochemical self-charging supercapacitor power cell using piezoelectrochemical spectroscopy, *Nat. Commun.*, 2020, **11**, 2351.
- 3 P. Pazhamalai, K. Krishnamoorthy, S. Sahoo, V. K. Mariappan and S.-J. Kim, Carbothermal conversion of siloxene sheets into silicon-oxy-carbide lamellae for high-performance supercapacitors, *Chem. Eng. J.*, 2020, **387**, 123886.
- 4 K. Krishnamoorthy, P. Pazhamalai and S.-J. J. Kim, Two-dimensional siloxene nanosheets: novel high-performance supercapacitor electrode materials, *Energy Environ. Sci.*, 2018, **11**, 1595–1602.
- 5 K. Krishnamoorthy, P. Pazhamalai and S. J. Kim, Ruthenium sulfide nanoparticles as a new pseudocapacitive material for supercapacitor, *Electrochim. Acta*, 2017, **227**, 85–94.
- 6 M. A. Bissett, I. A. Kinloch and R. A. W. Dryfe, Characterization of MoS₂-Graphene Composites for High-Performance Coin Cell Supercapacitors, *ACS Appl. Mater. Interfaces*, 2015, **7**, 17388–17398.
- 7 S. Sahoo, K. Krishnamoorthy, P. Pazhamalai, V. K. Mariappan, S. Manoharan and S.-J. Kim, High performance self-charging supercapacitors using a porous PVDF-ionic

- liquid electrolyte sandwiched between two-dimensional graphene electrodes, *J. Mater. Chem. A*, 2019, **7**, 21693–21703.
- 8 X. Xia, Y. Zhang, D. Chao, Q. Xiong, Z. Fan, X. Tong, J. Tu, H. Zhang and H. J. Fan, Tubular TiC fibre nanostructures as supercapacitor electrode materials with stable cycling life and wide-temperature performance, *Energy Environ. Sci.*, 2015, **8**, 1559–1568.
- 9 X. Lin, M. Salari, L. M. R. Arava, P. M. Ajayan and M. W. Grinstaff, High temperature electrical energy storage: advances, challenges, and frontiers, *Chem. Soc. Rev.*, 2016, **45**, 5848–5887.
- 10 J. L. Qi, X. Wang, J. H. Lin, F. Zhang, J. C. Feng and W.-D. Fei, Vertically oriented few-layer graphene-nanocup hybrid structured electrodes for high-performance supercapacitors, *J. Mater. Chem. A*, 2015, **3**, 12396–12403.
- 11 Z. Li, J. Liu, K. Jiang and T. Thundat, Carbonized nanocellulose sustainably boosts the performance of activated carbon in ionic liquid supercapacitors, *Nano Energy*, 2016, **25**, 161–169.
- 12 S. Pohlmann, T. Olyschläger, P. Goodrich, J. Alvarez Vicente, J. Jacquemin and A. Balducci, Azepanium-based ionic liquids as green electrolytes for high voltage supercapacitors, *J. Power Sources*, 2015, **273**, 931–936.
- 13 Y. Tao, X. Xie, W. Lv, D.-M. Tang, D. Kong, Z. Huang, H. Nishihara, T. Ishii, B. Li, D. Golberg, F. Kang, T. Kyotani and Q.-H. Yang, Towards ultrahigh volumetric capacitance: graphene derived highly dense but porous carbons for supercapacitors, *Sci. Rep.*, 2013, **3**, 2975.
- 14 Z. Liu, H. Zhang, Q. Yang and Y. Chen, Graphene / V₂O₅ hybrid electrode for an asymmetric supercapacitor with high energy density in an organic electrolyte, *Electrochim. Acta*, 2018, **287**, 149–157.

- 15 G. Sun, K. Li, L. Xie, J. Wang and Y. Li, Preparation of mesoporous carbon spheres with a bimodal pore size distribution and its application for electrochemical double layer capacitors based on ionic liquid as the electrolyte, *Microporous Mesoporous Mater.*, 2012, **151**, 282–286.
- 16 J. P. C. Trigueiro, R. L. Lavall and G. G. Silva, Supercapacitors based on modified graphene electrodes with poly(ionic liquid), *J. Power Sources*, 2014, **256**, 264–273.
- 17 B. Song, J. Zhao, M. Wang, J. Mullavey, Y. Zhu, Z. Geng, D. Chen, Y. Ding, K. Moon, M. Liu and C.-P. Wong, Systematic study on structural and electronic properties of diamine/triamine functionalized graphene networks for supercapacitor application, *Nano Energy*, 2017, **31**, 183–193.
- 18 Z. Lei, Z. Liu, H. Wang, X. Sun, L. Lu and X. S. Zhao, A high-energy-density supercapacitor with graphene-CMK-5 as the electrode and ionic liquid as the electrolyte, *J. Mater. Chem. A*, 2013, **1**, 2313–2321.
- 19 Y. Chen, X. Zhang, D. Zhang and Y. Ma, High power density of graphene-based supercapacitors in ionic liquid electrolytes, *Mater. Lett.*, 2012, **68**, 475–477.
- 20 N. das M. Pereira, J. P. C. Trigueiro, I. de F. Monteiro, L. A. Montoro and G. G. Silva, Graphene oxide – Ionic liquid composite electrolytes for safe and high-performance supercapacitors, *Electrochim. Acta*, 2018, **259**, 783–792.
- 21 K. Krishnamoorthy, P. Pazhamalai, V. K. Mariappan, S. Manoharan, D. Kesavan and S.-J. Kim, Two-Dimensional Siloxene–Graphene Heterostructure-Based High-Performance Supercapacitor for Capturing Regenerative Braking Energy in Electric Vehicles, *Adv. Funct. Mater.*, 2020, 2008422.
- 22 P. Pazhamalai, K. Krishnamoorthy, V. K. Mariappan, A. Sathyaseelan and S.-J. Kim, Solar driven renewable energy storage using rhenium disulfide nanostructure based rechargeable supercapacitors, *Mater. Chem. Front.*, 2020, **4**, 3290–3301.

- 23 P. Pazhamalai, K. Krishnamoorthy, S. Sahoo, V. K. Mariappan and S. J. Kim, Supercapacitive properties of amorphous MoS₃ and crystalline MoS₂ nanosheets in an organic electrolyte, *Inorg. Chem. Front.*, 2019, **6**, 2387–2395.
- 24 P. Pazhamalai, K. Krishnamoorthy, S. Sahoo and S. J. Kim, Two-dimensional molybdenum diselenide nanosheets as a novel electrode material for symmetric supercapacitors using organic electrolyte, *Electrochim. Acta*, 2019, **295**, 591–598.
- 25 P. Pazhamalai, K. Krishnamoorthy, V. K. Mariappan and S.-J. J. Kim, Blue TiO₂ nanosheets as a high-performance electrode material for supercapacitors, *J. Colloid Interface Sci.*, 2019, **536**, 62–70.
- 26 K. Krishnamoorthy, S. M. S. P., P. Pazhamalai, V. K. Mariappan, Y. S. Mok and S.-J. Kim, A highly efficient 2D siloxene coated Ni foam catalyst for methane dry reforming and an effective approach to recycle the spent catalyst for energy storage applications, *J. Mater. Chem. A*, 2019, **7**, 18950–18958.
- 27 A. Joshi, A. K. Tomar, G. Singh and R. K. Sharma, Engineering oxygen defects in the boron nanosheet for stabilizing complex bonding structure: An approach for high-performance supercapacitor, *Chem. Eng. J.*, 2020, 127122.
- 28 D. Kesavan, V. K. Mariappan, K. Krishnamoorthy and S.-J. Kim, Carbothermal conversion of boric acid into boron-oxy-carbide nanostructures for high-power supercapacitors, *J. Mater. Chem. A*, 2021, **9**, 915–921.
- 29 A. Burke, R&D considerations for the performance and application of electrochemical capacitors, *Electrochim. Acta*, 2007, **53**, 1083–1091.